CHAPTER 6 DRY SLIDING WEAR BEHAVIORS OF POWDER-THIXOCAST AL-25SI-2.5CU-1MG AND AL-20SI-5FE ALLOYS

6.1 Motivation

Hypereutectic Al-Si-X alloys are typically applied to where good wear resistance is preferably required. Hence, this Chapter will elucidate the wear characters of two powder-thixocast alloys, Al-25Si-2.5Cu-1Mg, and Al-20Si-5Fe.

This Chapter firstly briefs the fundamentals of metal wear. Metals behave complicatedly in wear. The wear behaviors depend not only on the material related parameters such as shape, size, composition and distribution of micro constituents, but also on the operating conditions such as load, sliding speed, temperature, environment and counter surfaces [45-70].

Like Chapter 5, two conventional alloys, LM13 and Al-25Si-2.5Cu-1Mg (IT), were also sliding tested for comparison with the powder-thixocast alloys. Experimental results indicate that the powder-thixocast alloys have much better wear resistance than the conventional alloys, especially when the wear tests were conducted in T6 conditions or sliding at high loads. Wearing mechanisms, based on the observations of worn surfaces and wears debris, to explain the wear results will also be proposed.

6.2 Introduction of metal wear

6.2.1 Types of metal wear

A well-defined wearing system must include not only the conditions of mutual contacting bodies, but also the environment and the interfacial element during wear [113]. Figure 6.1 depicts a wearing system typically consists of four elements: 1.solid body, 2. counterbody, 3. interfacial element, and 4. environment.

Several methods can be used to categorize the types of metal wear based on the four elements (Figure 6.1). For instance, wearing can take place under lubricating or

unlubricating (dry) conditions, in air or in humidity atmosphere, at room temperature or at elevated temperature, etc.

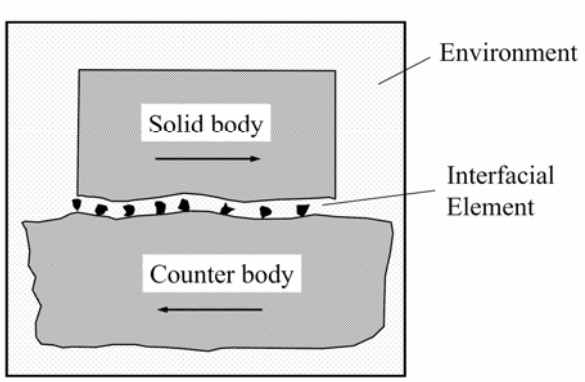

Figure 6.1 Schematic depiction of a wearing system [113].

Another way to categorize the types of wear is according to the relative motion between the body and counterbody, such as sliding, rolling, oscillating, impacting, and flowing, as shown in Figure 6.2.

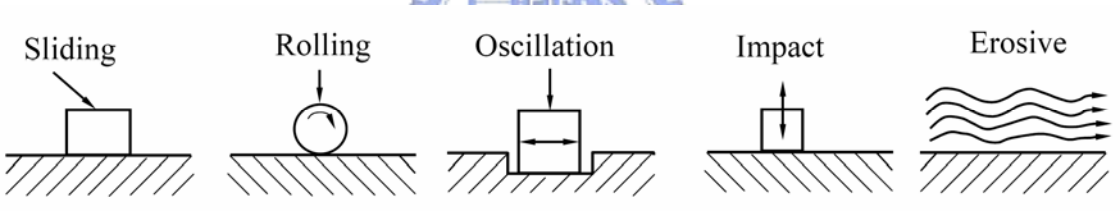

Figure 6.2 Classification of wear processes.[113]

6.2.2 Surface damages in sliding wear

In general, wearing surface damage is caused by the four mechanisms, adhesion, abrasion, tribochemical reactions, and surface fatigue, schematically shown in Fig. 6.3. The Al-Si-X alloys were found to be worn by these mechanisms, detailed in Sections 6.4 and 6.5.

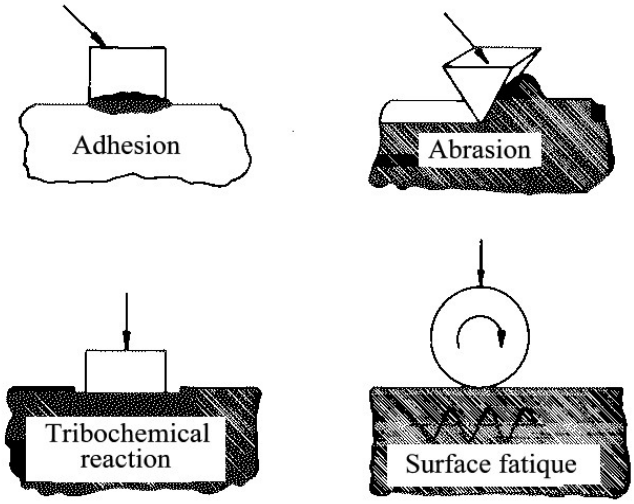

Figure 6.3 Schematic description of the four main wear mechanisms. [113]

Fig. 6.4 shows possible different physical processes which may occur in sliding wear [114]. Welded junctions are formed on clean mating surfaces due to adhesion (Fig. 6.4 a). As a result of relative motion, material is detached or transferred which can lead to grooving of softer asperities by the work-hardened transfer material. Sheet-like wear particles are formed, due to surface fatigue, during repeated plastic deformation by a harder conterbody (Fig. 6.4 b). Surface traction in sliding contact can lead to cracking of brittle materials such as ceramics (Fig. 6.4 c). Cracking of surface films formed by tribochemical reactions (Fig. 6.4 d) results in loose wear particles, which can act abrasively if they are harder than the base materials. Therefore, an understanding of the nature of the debris and the mixed layer from which the debris is formed, especially their microstructure and composition could provide important insight into the wear mechanisms of these materials.

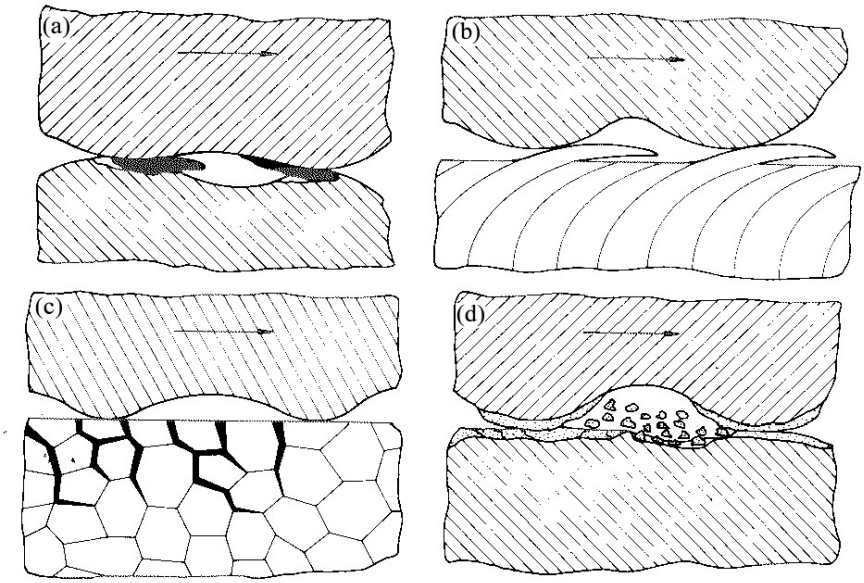

Figure 6.4 Mechanisms of wear during sliding contact

(a) adhesive junctions, material transfer and grooving, (b) surface fatigue due to repeated plastic deformation on ductile solids, (c) surface fatigue results in cracking on brittle solids and (d) tribochemical reaction and cracking of reaction films.[114]

6.2.3 Some theories about sliding wear of metals

A. Archard's adhesive wear theory

Adhesive wear of metals is the most often found under unlubricated or dry conditions. The most widely quoted adhesive wear theory is that of Archard [115], who proposed wear volume (W) is proportional to normal contact force (N) and sliding distance (L):

$$W = \left(\frac{K}{H}\right) N \bullet L$$

,where K is a constant and H is the hardness of sliding material. The value of K/H is called wear coefficient, with a unit of m^3/Nm, which is associated with sliding wear performance of a material in a specified wearing system.

A simple method for derivation of Archard's equation is schematically shown in Fig. 6.5. Note that the surface asperities will deform until the material yields sufficiently to carry the applied load. Hence, the pressure generated, P is equal to the yield stress, and this is referred to the hardness of the material, H.

In derivation of Archard's equation, assume that all adhesive junctions or asperities are semi-spheres with a radius 'a', as shown in Fig. 6.5. If there are 'n' junctions then the load carried will be: $N = n H\pi a^2$, i.e., the number of junctions will be: $n = N / H\pi a^2$. If *K* is the probability of break down of an adhering junction when the asperity moves forward in a sliding distance L='2a', than '*K*n' junctions will be broken and remade. Thus the total adhering wear volume will be: $W = Kn(2/3)(\pi a^3) = 2a/3K (N / H) = L N /(3 KH) = (K/H)NL$, let $K=3K$.

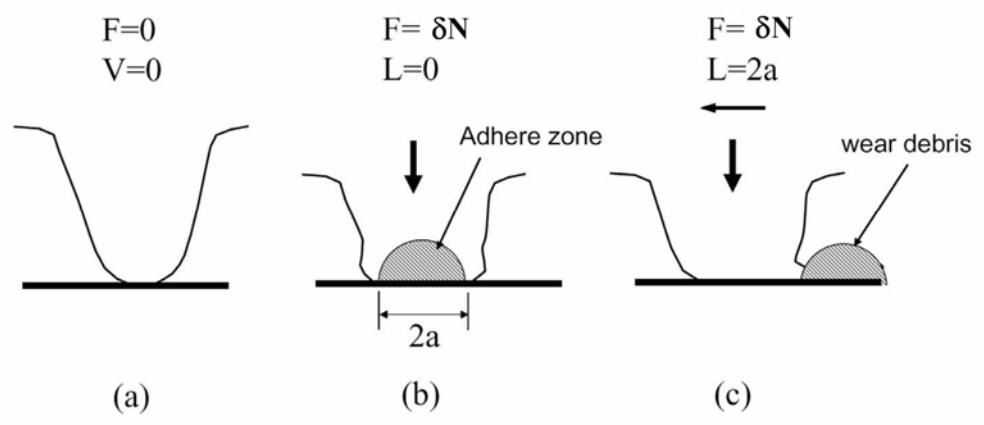

Figure 6.5 Schematic diagrams show Archard's adhere wearing model.

(a) An surface asperity statically contacts with a countersurface under no pressure, (b) under a normal force δN, and (c) after sliding a distance L=2a, where a is radius of the plastic deformation or adhering zone

B. Delamination theory of wear

Sheet-like wear debris of sliding surfaces may be caused by delamination mechanism. Delamination wear theory was first proposed by N.P. Suh [116,117]. This theory is based on dislocation theory and the plastic deformation and fracture of metals near a surface. In order to derive an equation to predict delaminating wear rate quantitatively, N.P. Suh made the following assumption:

(a) The worn metal was removed layer by layer, similar to the removal of skin from an onion. Each layer consists of N wear sheets (Fig.6.6).

(b) During wear, the material contact surfaces are plastically deformed, and dislocations are formed beneath the surface. However, at and very near the surface does not have a high dislocation density, due to the elimination of dislocations by escaping out of the worn surface. Therefore, a depth of dislocation free zone (or low dislocation zone) h is formed beneath the worn surface, leading to voids and cracks are formed at the distance h below the worn surface (Fig.6.7).

(c) The number of the wear sheets per layer is proportional to the number of asperities between the slider and the disk.

Using these assumptions, the wear rate W is derived as: W=κLS, where L is the load, S sliding distance, and κ is a wear factor given by

$$\kappa = \frac{b}{4\pi}\left[\frac{KG}{\sigma_f S_o(1-\nu)}\right]$$

where b is the Burgers vector, K is a constant, G the shear modulus, σ_f the friction stress, S_o is defined as the critical sliding distance required for removal of a layer, and ν is Poisson's ratio.

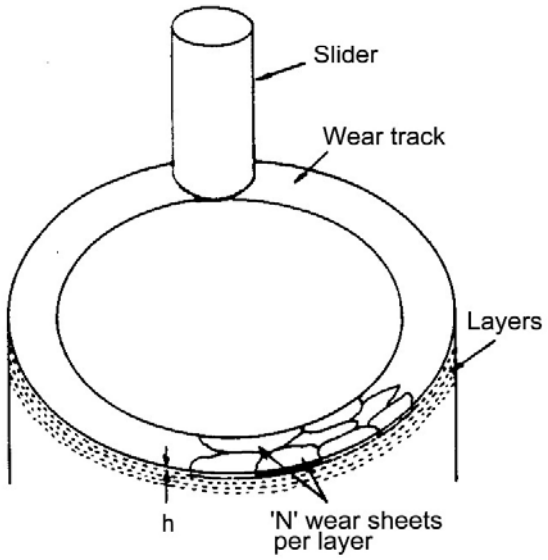

Figure 6.6 A schematic view of the metal being removed under a circular wear track in pin-on-disk type wear tests [116].

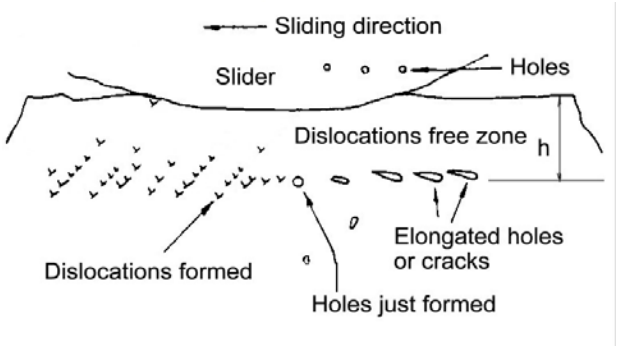

Figure 6.7 The process of wear particles formation by the shear deformation of the voids [116].

C. The model of Seizure

Seizure always occurs on sliding contact between two metal surfaces, if large-scale mass flow and metallic transfer begins to take place under abnormal sliding conditions. Physical explanation for metal seizure was provided by Tabor [118], and is briefly described in following.

Figure 6.8 illustrates an idealized model to explain how a seizure occurs between two sliding metal surfaces. When metal surfaces contact, the real area over which they touch, A_r , is usually very small. The contacting regions localize only on several points,

called asperities, due to surface roughness. Under static conditions, the contacting regions grow until the total area of regions A_r is large enough to support the load, as shown in Fig. a. As sliding speed and applied load increases, A_r increases, as shown in Fig. 6.8 b. Tabor [118] provided an equation to calculate the area A_r :

$$\left(\frac{F}{A_r}\right)^2 + \alpha s^2 = H^2$$

where F is the applied load, α is a constant value, s = $\mu F/A_r$, and H is the hardness of material. Tabor believed that when A_r grows under large enough loads and shearing rates to be equal to the nominal area, A_n, the sliding surfaces seize completely.

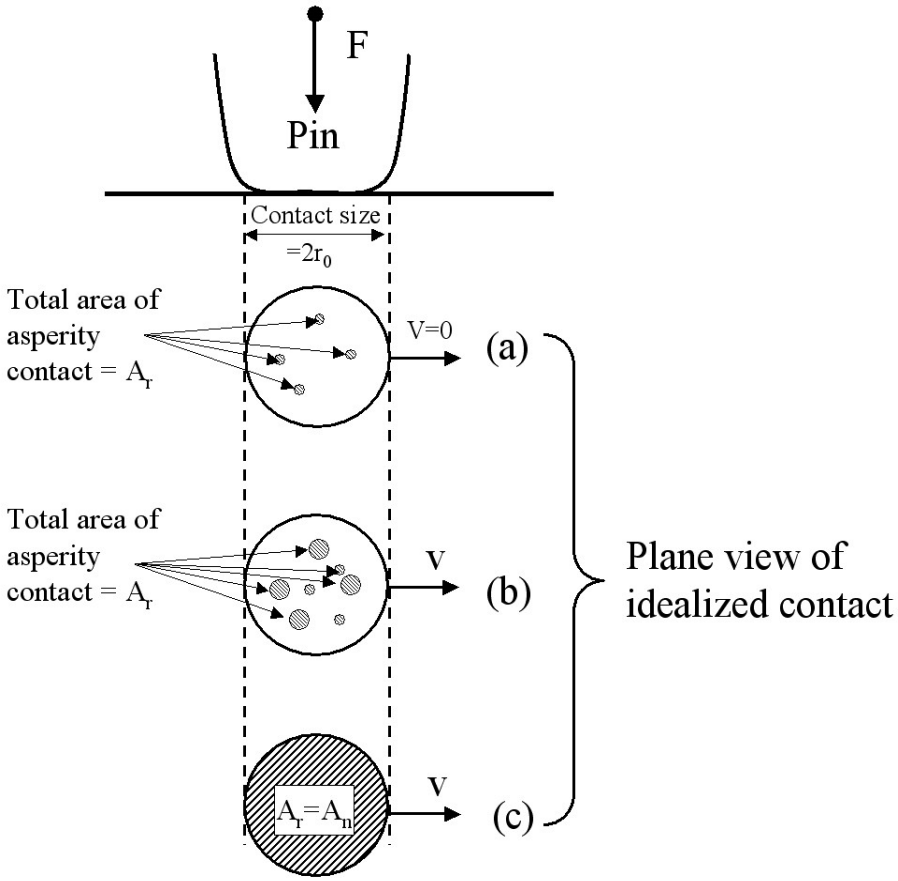

Figure 6.8 An idealized model for the seizure mechanism.

(a) The asperity contacts deform plastically, under the normal load F, until the real area of contact, Ar, is given by F/Ho. (b) Further increase in the normal load F and the presence of a tangential traction (v≠0) will increase the number of asperity contacts, N, as well as the size of each contact ro. The real area of contact, Ar, has increased. (c) Seizure take place when the area of contact, Ar, equals the nominal area of contact, An. [119]

D. Effect of second phases on wearing behaviors

Wear behavior can be markedly changed by embedding a second phase in a single-phase matrix, or by using a multiphase structure. Second phases can affect sliding wear by hardening of the matrix and/ or by reducing the real area of contact between a solid body and a counterbody. Depending on their identity, these phases can also cause effects such as changing the tendency for adhesion, changing the fatigue properties or the properties of transfer layers, or giving rise to abrasion.

Figure 6.9 displays different microstructures which are found in multiphase materials. Larger phases can form due to primary precipitation during cooling from the liquid states. These larger phases can be more effective in carrying the load imposed by the counterbody. For example, the hypereutectic Al-Si-X alloy examined herein contained a high volume fraction of larger primary crystals of silicon. These large particles can influence the wear behavior substantially.

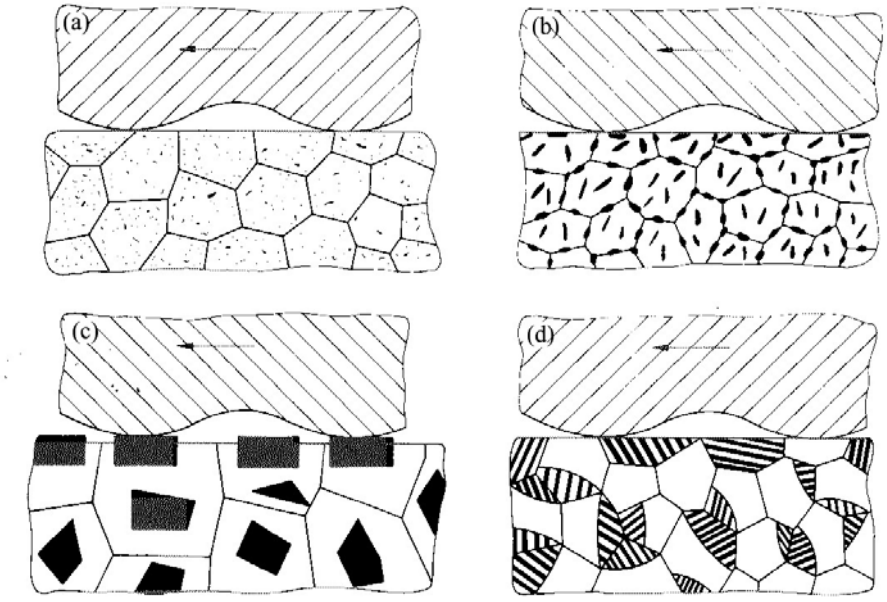

Figure 6.9 Schematic four types of second phase during sliding wear

Schematic representation of different multiphase structures showing (a) coherent and (b) incoherent particles in precipitation- hardened alloys, (c) large primarily precipitated particles or constituents of composites, (d) two-phase structures of eutectic or eutectoid systems. [114]

E. Effect of load, speed and environmental condition

Sliding wear is strongly influenced by load, sliding speed and environmental conditions such as temperature, humidity, partial oxygen pressure, etc. Wear as a function of operating time or sliding distance depends on the predominant wear mechanism. According to Fig.6.10, three different periods can be distinguished in the wear loss/ operating time curves. The running-in period I is followed by the steady-state period II, which finally goes over to the breakdown period.

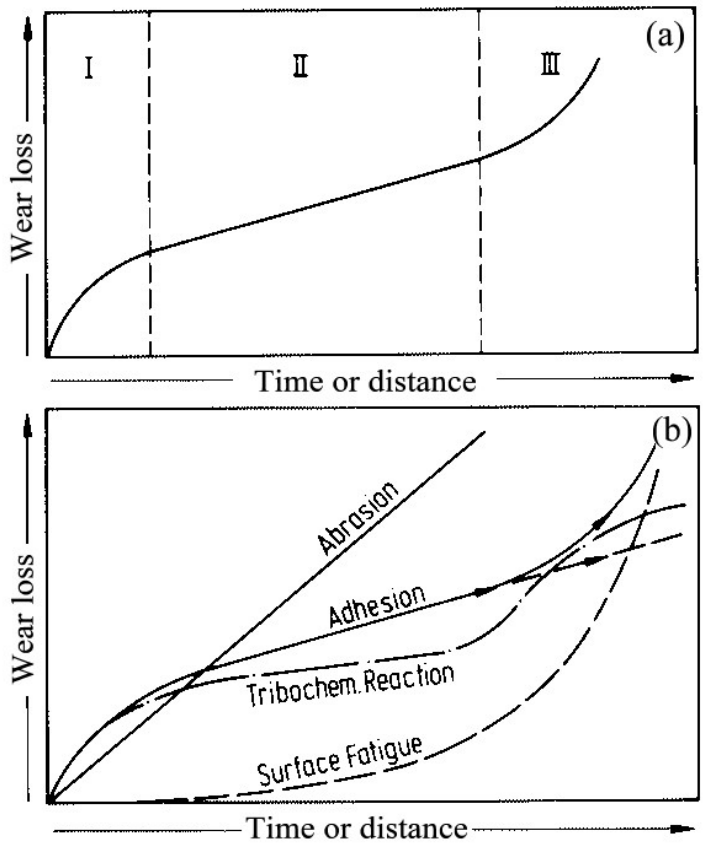

Figure 6.10 Typical wearing curves show different wearing stage [114]

6.3 Experimental

6.3.1 Materials

Four alloys were used in this study. Two powder-thixocast alloys, referred to Al-25SiCuMg (PT) and Al-20SiFe (PT), have nominal compositions of

Al-25Si-2.5Cu-1Mg and Al-20Si-5Fe respectively. Two conventional alloys, referred to Al-25SiCuMg (IT) and LM13 (in BS standard or AC8A in JIS standard), have nominal compositions of Al-25Si-2.5Cu-1Mg and Al-12Si-1Cu-1Mg respectively. Fabrication procedures of these alloys are the same as those described in Chapter 5.

6.3.2 Sliding wear tests

Wear tests were performed using a conventional pin-on-disc testing machine, as is schematically illustrated in Fig. 6.11. A pin specimen bearing a load is held by a fixture that mounted at one end of a bar. The fixture enables the pin to freely move up and down. The bar is supported at its midpoint by a bearing so that the bar can freely rotate. A load cell is attached to the other end of the bar to record the friction traction during sliding.

The pins with flat ends, 8 mm in diameter and 15 mm long, were machined from the thixocast or cast Al-Si-X alloys. The disc-shaped counter material was BS 708 M40 steel whose hardness was adjusted by heat-treatment to Rockwell C 40.

All tests were performed in air, without lubricant and at room temperature. Before the wearing test, the surfaces of the aluminum alloy pins and the counterface disc were polished to a surface roughness, Ra, of under 0.1μm. During the wearing test, the applied load was increased stepwise until the onset of specimen seizure was noted. The specimen seizure was specified by the abnormal noise in the pin-disc assembly and the strong adhesion of the specimen material to the disc. At each step in the wearing test, the pin was slid at a constant speed of 1.57 m s^{-1} over a distance of 1.88 km under constant load. At the end of each step, the rotation of the steel disc was stopped automatically and a surface thermal couple was immediately employed to measure the bulk temperature of the pin by touching the worn surface of the pin. Then, the worn pin was withdrawn from the fixture of the wear machine and was weighed to determine the wear rate. After an interval of about 5 minutes, the same pin that had been worn and weighed was used again in the next step for the wearing test. The wear rate values were determined from the measured weight loss and expressed in terms of volume loss per unit sliding distance (m^3 per m). Each wear rate value was averaged from the data obtained on at least two wearing pins.

The worn surfaces and debris after sliding at different loads were investigated by XRD, SEM and EDS. Subsurface microstructures were also investigated at the cross-sections perpendicular to the worn surface. Microstructures were observed using optical microscope, and samples were etched using 0.5%HF water solution. Surface roughness values of pins and discs were measured before and after sliding using MITUTOYO SURFTEST, a surface roughness measuring instrument.

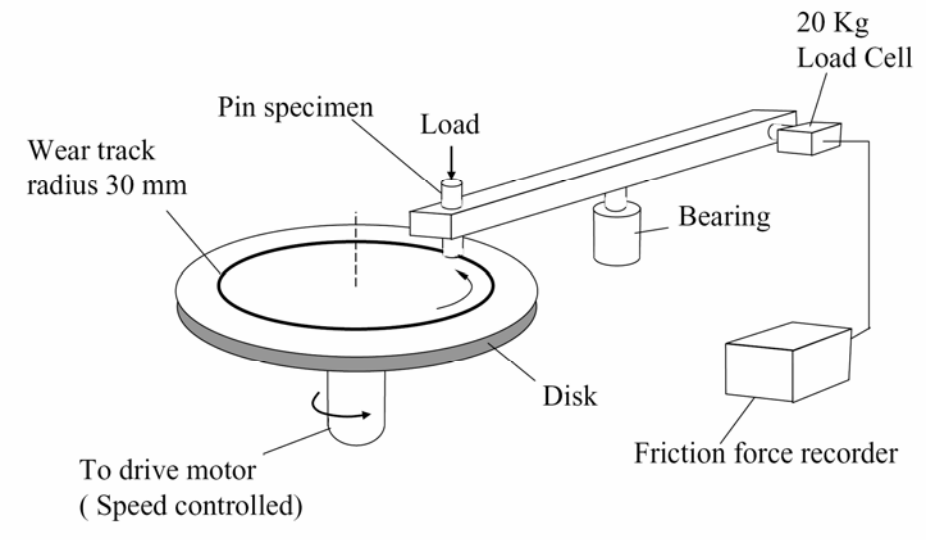

Figure 6.11 Schematic illustration of pin-on-disk friction testing apparatus

6.4 Results

6.4.1 Wear rate and coefficient of friction

Figures 6.12 a and b plots the wear rates as a function of applied sliding load for the Al-Si-X alloys in as-prepared and T6-treated states, respectively. At low loads, as-prepared Al-25SiCuMg (PT) and (IT) have smaller wear rate than LM13 and Al-20SiFe (PT) alloy; whereas at high loads, as-prepared Al-25SiCuMg (PT) showed much lower wear rate than did the conventional alloys- Al-25SiCuMg (IT) and LM13 (Fig.6.12a).

Following T6 treatment, all the Al-Si-Cu-Mg alloys except Al-25SiCuMg (IT) showed improved wear resistance (comparing Fig. 6.12 a with b). The effects of T6 treatment on the wear resistances of Al-25SiCuMg (PT) and Al-25SiCuMg (IT) alloys differed, although the two alloys were similarly composed. T6 treatment greatly increased the wear resistance of Al-25SiCuMg (PT) alloy, but reduced that of Al-25SiCuMg (IT) alloy, even though it increased the microhardness of Al-25SiCuMg (IT) alloy (Hv 152 against 108 in Table 2 in Chapter 5). Figure 6.12 also reveals that Al-25SiCuMg (PT) had the highest seizure resistance in both as-cast and T6 state. And, LM13 alloy (~12wt%Si) had a lower seizure resistance than hypereutectic Al-25SiCuMg (PT) and (IT) alloys ($>$12wt%Si).

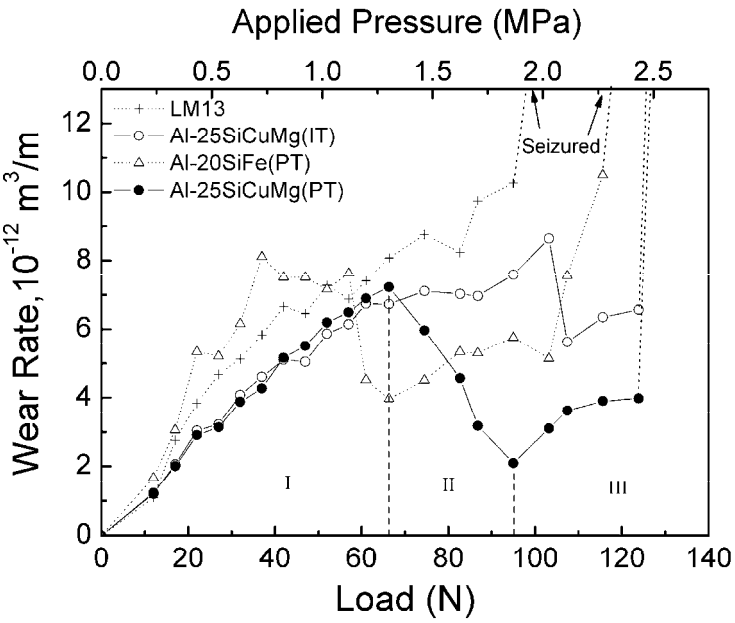

(a)

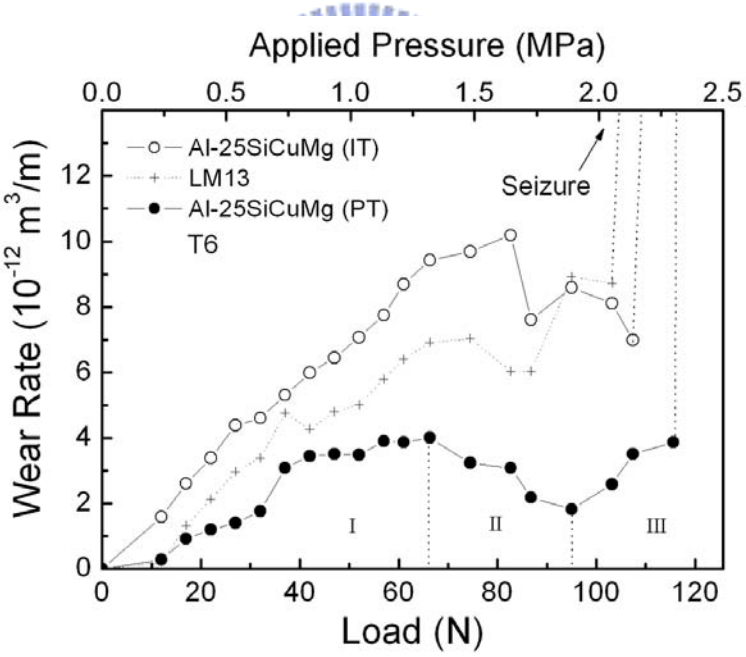

(b)

Figure 6.12 Wear rates varied with load for the (a) as-prepared and (b) T-treated Al-Si-X alloys. The three regions denoted by I, II, and III are shown for Al-25SiCuMg (PT) alloy.

Coefficients of friction during sliding tests were continuously recorded using a computer. Figure 6.13 presents two examples of the measured results for as-prepared Al-25SiCuMg (PT) and LM13 alloys. As the wear tests progressed, the coefficients of friction soon reach to a stable value of about 0.5 (region I in Fig. 6.13). When the applied load was further increased beyond around 67N, the coefficient for Al-25SiCuMg (PT) fist increased than decreased (Fig. 6.13a), however, the coefficient of LM13 only declined (Fig. 6.13b). This seems to indicate that LM13 do not have the region II like that exists in Al-25SiCuMg (PT).

A series of figures like that in Fig. 6.13 yields the mean coefficients of friction, which vary with the load for various alloys. Figure 6.14 plots the variations in such coefficients.

The coefficients of friction at low loads (region I in Fig. 6.12) substantially follow the order, LM13>Al-25SiCuMg (PT)> Al-25SiCuMg (IT), for both the as-prepared and the T6-treated Al-Si alloys. All the coefficients of friction of the as-prepared and T6-treated Al-Si-Cu-Mg alloys exhibited a transition from stable to unstable states at a load of approximately 67N (Figs. 6.12 a and b). The T6-treated alloys exhibited lower coefficients of friction than the as-prepared alloys (comparing Fig. 6.12 b with a).

From Figs. 6.12 to 6.14, wear behaviors depending on applied load observed for Al-25SiCuMg (PT) and Al-20SiFe (PT) alloys clearly show three regions, denoted by I, II, and III in these figures. In region I, the wear rate for the two alloys increased almost linearly with the load (Figs. 6.12); meanwhile, their coefficient of friction remained almost constant (Figs. 6.14). In region II, their wear rate began to fall as the load increased to about 67N for Al-25SiCuMg (PT) (Figs. 6.12); meanwhile, the coefficient of friction came to increase with the load (Figs. 6.14). This trend was followed by region III where wear rates increased and the coefficient of friction decreased. Finally, the specimen underwent seizure. From Figs. 6.12 and 6.14, the wear regions II and III can be apparent on the powder-thixocast alloys, however, they are not evident on the conventional alloys, Al-25SiCuMg (IT) and LM13.

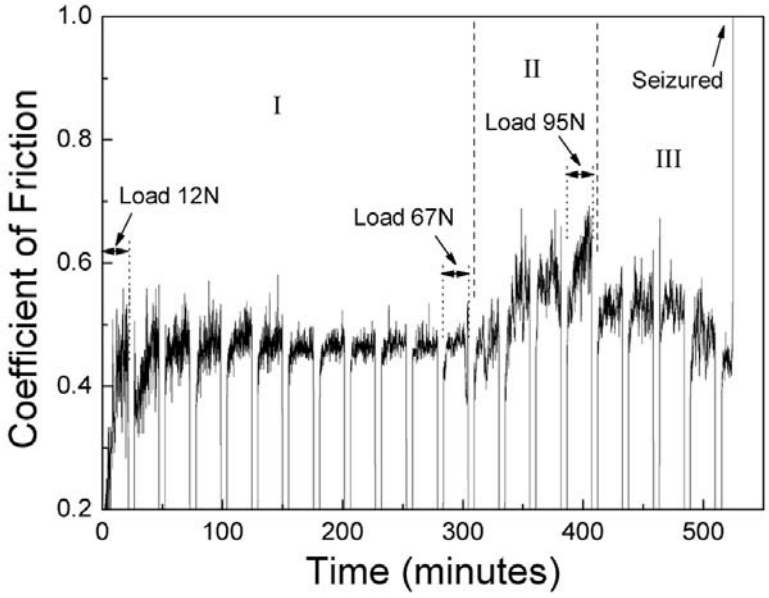

(a)

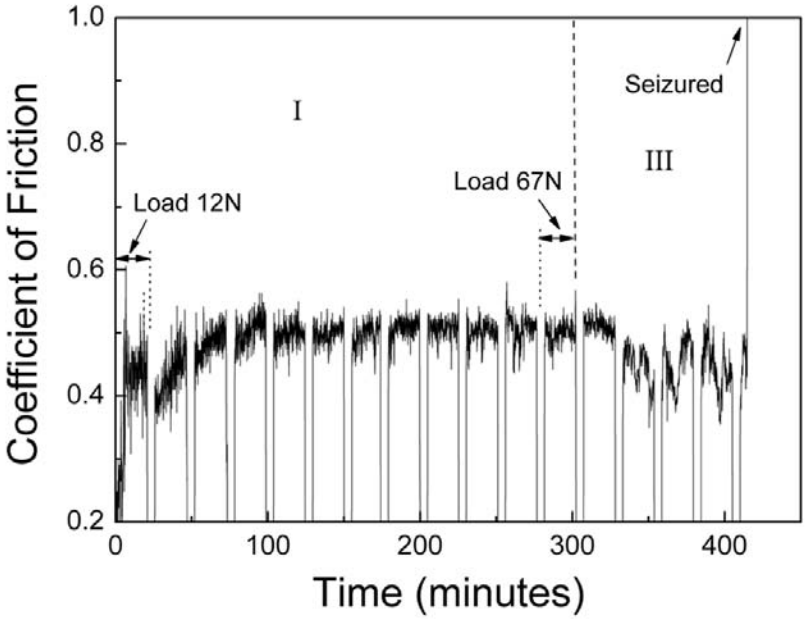

(b)

Figure 6.13 Coefficients of friction varied with sliding time for as-prepared (a) Al-25SiCuMg (PT) and (b) LM13 alloys.

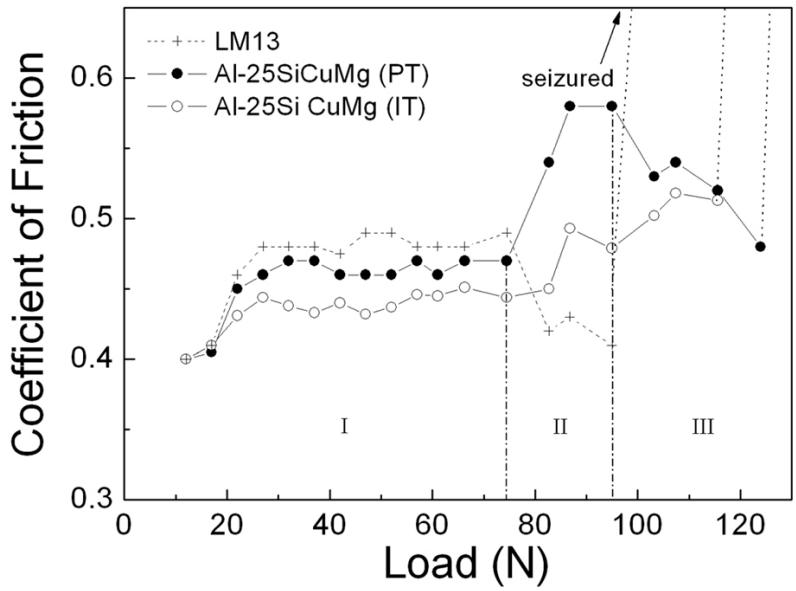

(a)

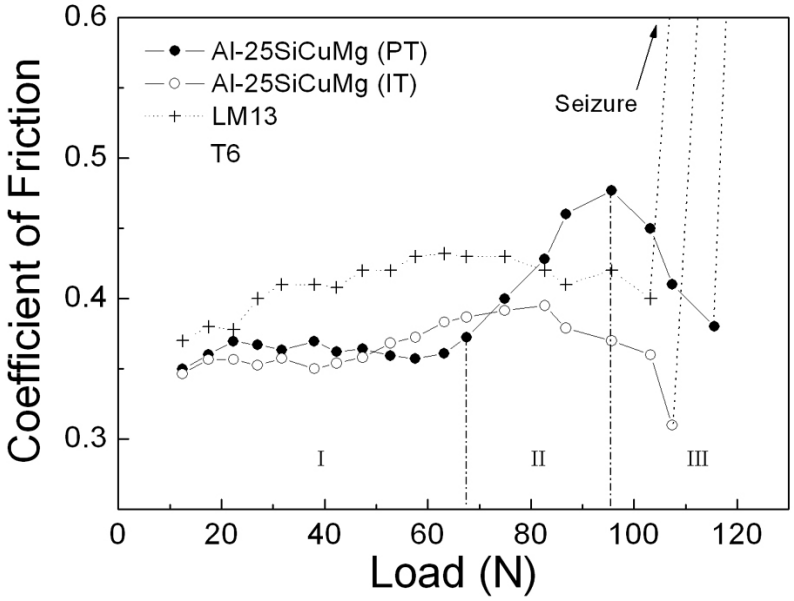

(b)

Figure 6.14 Coefficients of friction varied with load for (a) as-prepared and (b) T6-treated Al-Si-X alloys.

6.4.2 Surface roughness of discs and pins after wearing

Figure 6.15 shows the photographs of disc surfaces after seizure occurred on sliding contact with Al-Si-X alloy pins. Almost no sticky aluminum was found to be transferred from both as-prepared and T6-treated Al-25SiCuMg (PT) and (IT) alloys to the disc counter surfaces; whereas, a large amount of aluminum is found to be transferred from LM13 alloy pin to the disc surface. This result may be attributed to the primary Si particles in Al-25SiCuMg alloys, reducing the opportunity of aluminum matrix stick to the steel discs during sliding contact.

Surface roughness profiles of each pair of sliding pin and disc after seizure were measured. Figure 6.16 show the examples of the measuring results, and all the measured data are expressed in Ra and listed in Table 6.1. Roughness value Ra is defined as,

$R_a = \frac{1}{L}\int_0^L |f(x)|dx$, where L is the measure length and f(x) is the roughness curve.

These data agree with Figure 6.15, which shows that LM13 alloy has highest roughness on both surfaces of pin and disc, due to the material transfer. However, even in case of no material transfer, Al-25SiCuMg (PT) is found to have lower surface roughness than do Al-25SiCuMg (IT). This may indicate that fine and uniform primary Si particles in the former alloy have the advantages in reducing surface scrapes during sliding wear.

Table 6.1 Surface roughness values (Ra, μm) measured on the worn pins and discs after seizure

	Al-25SiCuMg (PT)		Al-25SiCuMg (IT)		Al-20SiFe (PT)	LM13	
	as-thixocast	T6	as-thixocast	T6	as-thixocast	as-cast	T6
pin	5.7	6.3	7.2	7.4	8.5	20.5	12.7
disc	1.0	0.7	1.2	1.4	1.3	1.7	1.4

*Surface roughness of disc before sliding test were 0.22 (Ra, μm).

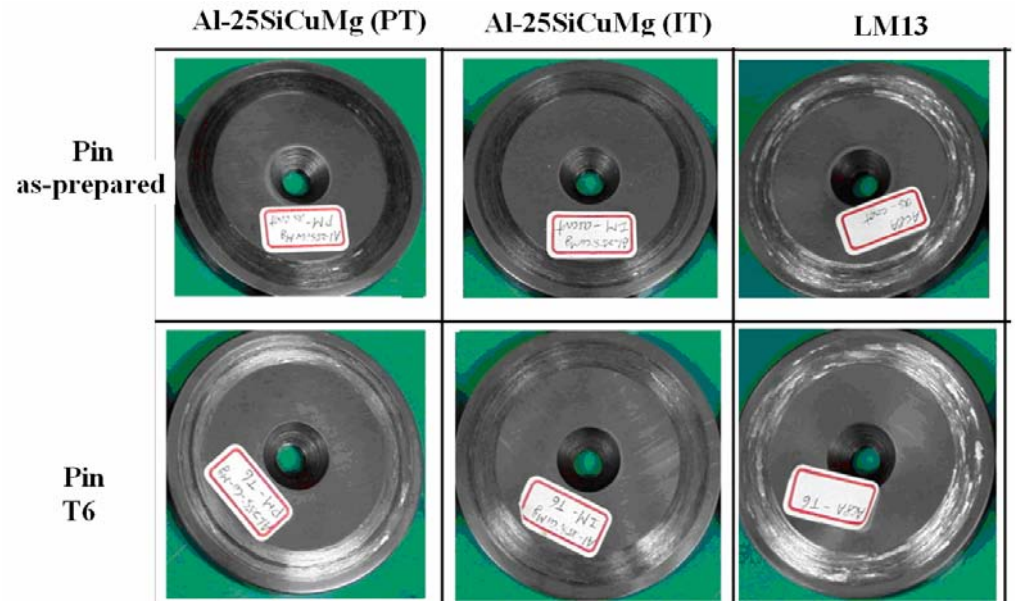

Figure 6.15 Photographs of the disc after sliding wear tests.

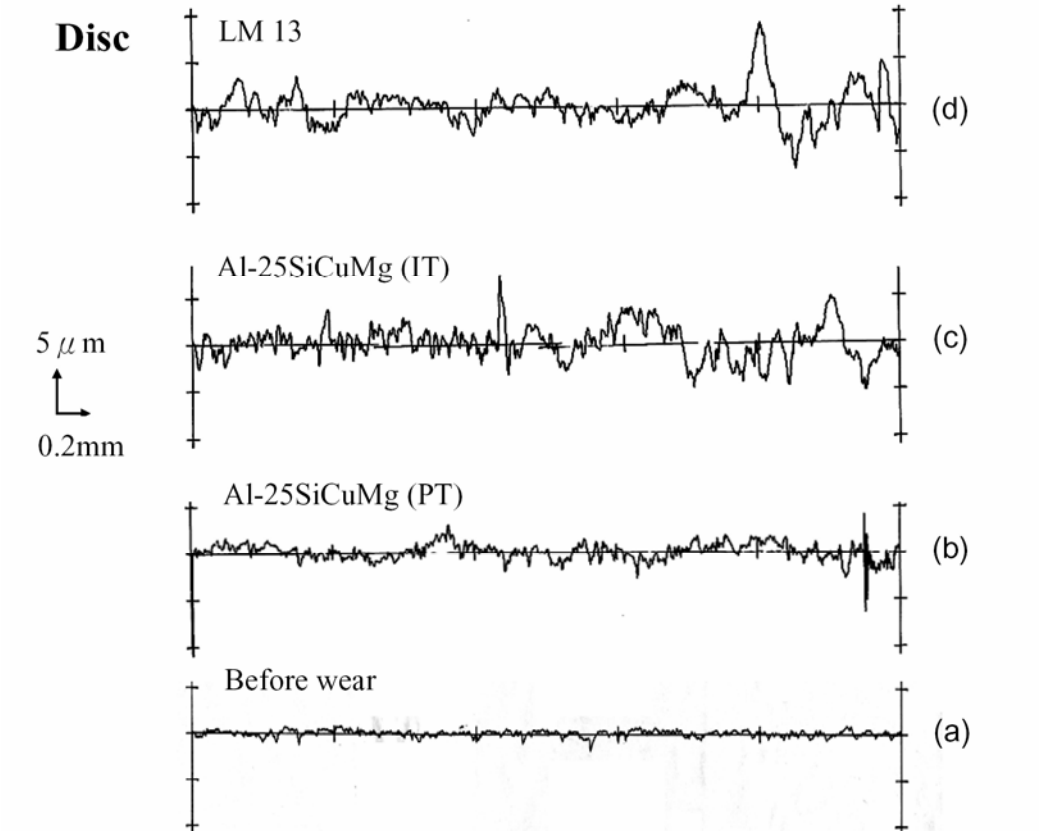

Figure 6.16 Surface roughness curves of discs (a) before wearing, (b) after sliding with Al-25SiCuMg (PT), (c) Al-25SiCuMg (IT), and (d) LM13 T6-treated alloys.